JACS
JOURNAL OF THE AMERICAN CHEMICAL SOCIETY

Article

pubs.acs.org/JACS

Supramolecular Photochirogenesis with a Higher-Order Complex: Highly Accelerated Exclusively Head-to-Head Photocyclodimerization of 2-Anthracenecarboxylic Acid via 2:2 Complexation with Prolinol

Yuko Kawanami,[†] Shin-ya Katsumata,[†] Masaki Nishijima,[‡] Gaku Fukuhara,[†] Kaori Asano,[§] Takeyuki Suzuki,[§] Cheng Yang,[†,⊥] Asao Nakamura,[∥] Tadashi Mori,[†] and Yoshihisa Inoue*[,†]

[†]Department of Applied Chemistry and [‡]Office for University−Industry Collaboration, Osaka University, Yamadaoka, Suita 565-0871, Japan

[§]Comprehensive Analysis Center, Institute of Scientific and Industrial Research, Osaka University, Mihogaoka, Ibaraki 567-0047, Japan

[⊥]Key Laboratory of Green Chemistry & Technology (Ministry of Education), College of Chemistry, Sichuan University, Wangjiang Road, Chengdu 610064, China

[∥]Department of Chemistry, College of Engineering, Shibaura Institute of Technology, Saitama-shi 337-8570, Japan

Supporting Information

ABSTRACT: An unprecedented 2:2 complex was shown to intervene in the enantiodifferentiating photocyclodimerization of 2-anthracenecarboxylic acid (**A**) mediated by a hydrogen-bonding template L-prolinol (**P**) to accelerate the formation of chiral *anti-head-to-head* and achiral *syn-head-to-head* cyclodimers in >99% combined yield with enhanced enantioselectivities of up to 72% ee for the former. The supramolecular complexation and photochirogenic behaviors, as well as the plausible structures, of intervening $\mathbf{A}_m\cdot\mathbf{P}_n$ complexes (m, n = 1 or 2) were elucidated by combined theoretical and experimental spectroscopic, photophysical, and photochemical studies. Furthermore, the photochemical chiral amplification was achieved for the first time by utilizing the preferential 2:2 complexation of **A** with homochiral **P** to give normalized product enantioselectivities higher than those of the template used. The present strategy based on the higher-order hydrogen-bonding motif, which is potentially applicable to a variety of carboxylic acids and β-aminoalcohols, is not only conceptually new and expandable to other (photo)chirogenic and sensing systems but also may serve as a versatile tool for achieving photochemical asymmetric amplification and constructing chiral functional supramolecular architectures.

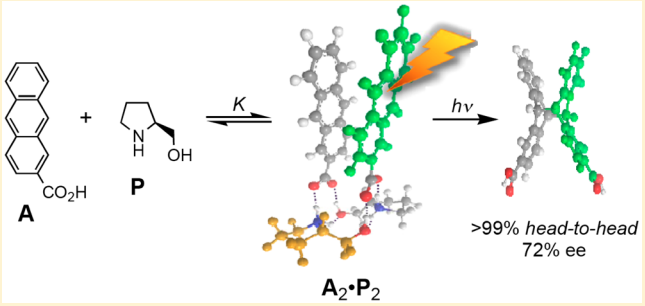

INTRODUCTION

Possessing several unique features complementary to the thermal counterpart, photochemical asymmetric synthesis, or photochirogenesis, has attracted much attention in the last two decades.[1] Controlling the stereochemical fate of a short-lived, weakly interacting excited-state species is, however, a challenging task and has rarely been achieved at a high level in isotropic solution.[1] Supramolecular photochirogenesis, benefiting from the synergetic chirogenic interactions in ground and excited states, is often advantageous over the conventional "molecular" strategy that exploits only the excited-state interactions and hence has attracted growing interest particularly in recent years.[2] Indeed, a number of photochirogenic transformations have been mediated by chiral inorganic, organic, and biomolecular hosts and templates to afford enantio- and diastereomeric products in moderate to high optical yields.[2] These supramolecular mediators may be classified into two categories by the complexity of host architecture and complexation/photochirogenesis strategy. Thus, structurally more sophisticated *confining hosts* possess a well-defined three-dimensional chiral cavity, and the inclusion complexation and subsequent photoreaction are stereochemically controlled by an array of noncovalent interactions, while synthetic or semisynthetic *hydrogen-bonding templates* usually possess a fence to shield one of the enantiotopic faces of a prochiral substrate upon complexation by two or more hydrogen bonds, facilitating attack from the open face. Although both strategies have been successful in terms of the enantioselectivity achieved,[2] the chiral template approach may have some practical advantages: (1) the antipodal product is readily obtained by switching the chiral sense of the template;

Received: June 1, 2016
Published: August 9, 2016

DOI: 10.1021/jacs.6b05598
J. Am. Chem. Soc. 2016, 138, 12187−12201

Scheme 1. Enantiodifferentiating Photocyclodimerization of 2-Anthracenecarboxylic Acid (A) Mediated by L-Prolinol (P), *N*-Methyl- (P_{NM}) and *O*-Methyl-L-prolinol (P_{OM}), TKS159 (T), and TM166 (TM)

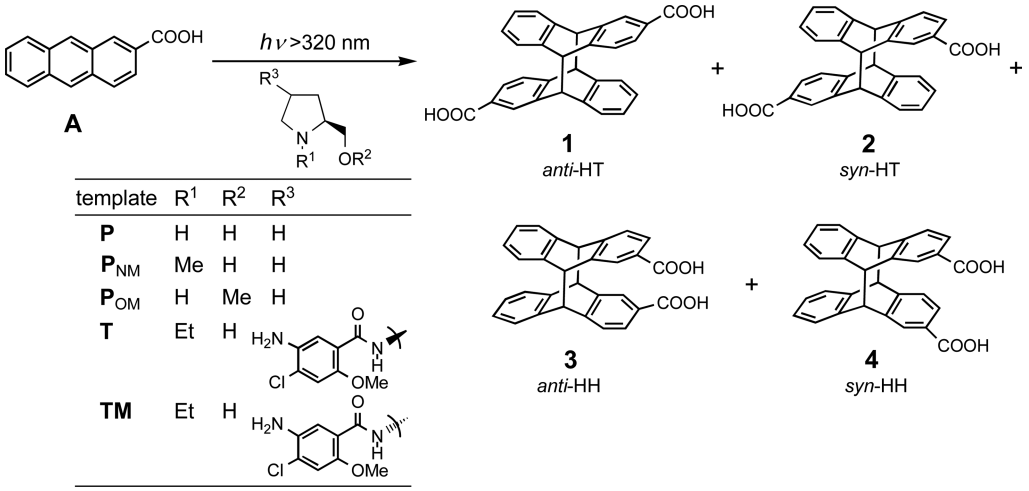

template	R^1	R^2	R^3
P	H	H	H
$\mathbf{P_{NM}}$	Me	H	H
$\mathbf{P_{OM}}$	H	Me	H
T	Et	H	
TM	Et	H	

(2) the mechanistic elucidation at the molecular level is more straightforward; (3) the theoretical calculations provide a plausible structure for the precursor complex; (4) the rational design to improve enantioselectivity is feasible; and (5) the strategy does not rely on size/shape matching and is potentially more expandable to other substrates.

A variety of chiral hydrogen-bonding templates, including Kemp's triacid derivatives,[3] α,α,α′,α′-tetraaryl-2,2-dimethyl-1,3-dioxolane-4,5-dimethanol derivatives (TADDOLs),[4] *N*-pyridyl-isophthalamides with a benzophenone moiety,[5] 2-methoxybenzamide derivatives of 4-aminoprolinol,[6] binaphthyl(thio)ureas,[7] and *trans*-1,2-diaminocyclohexane-based bis(thiourea)s[8] have hitherto been proposed and examined as mediators for enantiodifferentiating photocyclization, [2 + 2] and [3 + 2] photocycloadditions, and [4 + 4] photocyclodimerization reactions, all of which take advantage of the stoichiometric 1:1 template−substrate complexation. Thus, Bach et al.[3] developed chiral lactam templates derived from the Kemp's triacid and applied them to various enantiodifferentiating photocyclization and [2 + 2] photocycloaddition reactions to achieve high enantiomeric excesses (ee's) of up to 99%.[3e] Porco et al.[4] demonstrated that the enantiodifferentiating [3 + 2] photocycloaddition of 3-hydroxyflavone to methyl cinnamate is mediated by TADDOLs to give cycloaddition−rearrangement products in up to 89% ee at −70 °C. Krische et al.[5] employed a sensitizing hydrogen-bonding template with a benzophenone moiety for intramolecular [2 + 2] photocycloaddition of 3-butenyl quinolonyl ether to obtain a cyclobutane derivative in 19−22% ee at −70 °C. More recently, Sivaguru et al. employed binaphthol-attached ureas and thioureas as chiral templates for mediating the intramolecular [2 + 2] photocycloaddition of butenylcoumarins to obtain high ee's of up to 96%,[7] while Bach et al. demonstrated that (1*R*,2*R*)-1,2-diaminocyclohexane-based bis(thiourea)s mediate the intramolecular [2 + 2] photocycloaddition of *N*-butenoyldihydropyridone to afford cycloadducts in ee's of up to 76%.[8]

We also have shown that the enantiodifferentiating [4 + 4] photocyclodimerization of 2-anthracenecarboxylic acid (**A**) is mediated by 4-amino-5-chloro-2-methoxy-*N*-((2*S*,4*S*)-(1-ethyl-2-hydroxymethyl-4-pyrrolidinyl))benzamide (TKS159 or **T**) to afford a mixture of four stereoisomeric cyclodimers **1**−**4** (Scheme 1) through the 1:1 hydrogen-bonding complex of **A** with **T**. In this reaction, chiral *syn-head-to-tail* (*syn*-HT) and *anti-head-to-head* (*anti*-HH) cyclodimers **2** and **3** were obtained in 43−49% ee in dichloromethane at −50 °C.[6a,b] Intriguingly, the circular dichroism (CD) spectral Job analyses performed at different total concentrations (0.3 and 0.75 mM) afforded entirely different plots, exhibiting obvious deviations from the 1:1 stoichiometry at high **A** fractions for the run at 0.75 mM.[6c] Furthermore, upon irradiation of **A** (0.25 mM) with **T** (0.06−30 mM), the ee of **3** obtained, which should be identical to that of **2** if a single precursor **A**−**T** complex intervened, was substantially lower than that of **2** at intermediate **A**/**T** ratios. Detailed CD spectral and product analyses revealed the existence of 2:1 complex ($\mathbf{A_2}\cdot\mathbf{T}$) formed through the weak hydrogen-bonding association of the 1:1 complex (**A**·**T**) with additional **A** at K_2 = 100 M^{-1} (in CH_2Cl_2 at 25 °C), which is much smaller than K_1 = 3400 M^{-1} obtained for the 1:1 complexation.[6c] Although $\mathbf{A_2}\cdot\mathbf{T}$ is only a very minor component (≤1% of the total **A** species in the solution), two HH-oriented **A** molecules in $\mathbf{A_2}\cdot\mathbf{T}$ greatly accelerate the intracomplex photocyclodimerization to **3** and **4**, but the ee of **3** thus produced is much lower than that derived from the intermolecular photocyclodimerization of **A**·**T**, probably due to the weakly bound, and hence conformationally flexible, second **A** in $\mathbf{A_2}\cdot\mathbf{T}$.

In the 1:1 complex of **A** with **T**, the *N*-ethylprolinol moiety of **T** captures **A** by forming a nine-membered hydrogen-bonding network,[6a] while the benzamide moiety preferentially shields the enantiotopic *si* face of **A** to afford the *P*-enantiomer of **3** in up to 49% ee upon attack from the exposed *re* face by free **A** or **A**·**T** in the excited state.[6b,c,9] It is likely therefore that any template that lacks the shielding fence leads to poor enantioselectivity. Indeed, hydrogen-bonding template TM166, which is epimeric to **T** at the prolinol's 4-position and hence favors the extended conformation, gave racemic **2** and **3**.[6a] Nevertheless, we wanted to examine the binding and photochirogenic abilities of L-prolinol (**P**), the essential hydrogen-bonding chiral moiety of **T**, simply due to its ability to anchor two **A** molecules in a head-to-head manner in the $\mathbf{A_2}\cdot\mathbf{T}$ complex. This exploratory investigation with a simple β-aminoalcohol template, **P**, led us to very unexpected CD spectral and photochirogenic behaviors of **A**, which are explainable only by postulating complicated complexation equilibria of **A** with **P**, involving not only 1:1 and 2:1 but also 1:2 and 2:2 complexes. In the present study, we will first

DOI: 10.1021/jacs.6b05598
J. Am. Chem. Soc. 2016, 138, 12187−12201

reveal the structural conditions indispensable for this novel hydrogen-bonding motif by examining a series of modified **P** and then elucidate the factors and mechanisms that enable the higher-order hydrogen-bonding complexation and the exclusively head-to-head photocyclodimerization of **A** with enhanced rate and enantioselectivity.

RESULTS AND DISCUSSION

Stoichiometric 1:1 Complexation. We first examined the complexation behavior of **A** with **P** by UV/vis spectral titration and Job analysis; for the possible contribution of dual hydrogen-bonded dimer of **A**, see Figure S1 and Table S1 (for figures and tables with prefix S, see the Supporting Information) and relevant discussion. As illustrated in Figure 1

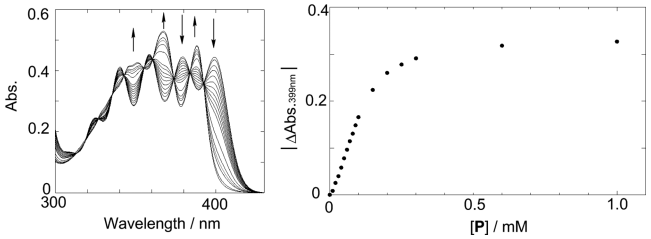

Figure 1. Left: UV/vis spectra of **A** (0.1 mM) in the presence of **P** (0–10 equiv) in CH_2Cl_2 at 25 °C. Right: Absorbance changes monitored at 399 nm as a function of [**P**].

(left), the ^1L_a and ^1L_b bands of **A** (0.1 mM) hypsochromically shifted with accompanying apparent isosbestic points upon stepwise addition of **P** (0–10 equiv) in dichloromethane at 25 °C, suggesting rather straightforward 1:1 complexation. The hypsochromic shifts are attributable to the deprotonation of **A** upon interaction with **P** since anionic **A** prepared in basic ethanol[10a] or in aqueous buffer solution at pH 9[10b] shows similar spectra with comparable hypsochromic shifts. The Job plot performed at a total concentration of 0.35 mM also gave a clear peak at a molar fraction of **A** (x) = 0.5, indicating the 1:1 stoichiometry, as shown in Figure S2. However, a closer inspection of the titration curve (Figure 1, right) revealed the sigmoidal nature at low **P** concentrations, implying formation of complex(es) containing multiple **A**s at high **A**/**P** ratios.

Hence, we deemed the UV/vis spectral titration at [**A**] = 0.1 mM unsuitable for the quantitative evaluation of the equilibrium constant for 1:1 complexation (K_{11}) free from the contamination by higher-order complexes. Instead, we performed the fluorescence spectral titration at [**A**] = 25 μM. Upon addition of **P** (0–10 equiv), the fluorescence intensity of free **A** gradually decreased and a new emission appeared at shorter wavelengths (around 390 nm) with an accompanying isoemissive point at 410 nm (Figure 2), which is attributable to the fluorescence of the **A**·**P** complex, as the excitation spectrum monitored at 441 nm was consistent in shape with the UV/vis spectrum obtained at high **P**/**A** ratios (Figure S3). Since the excitation wavelength was set at one of the isosbestic points (i.e., 355 nm; see Figure 1), the relative fluorescence efficiency of **A**·**P** versus **A** is evaluated as ca. 0.5 by comparing the integrated fluorescence intensities of the two species at the same concentration (see Figure S4). The lower fluorescence efficiency for **A**·**P** seems reasonable in view of the presence of an additional vibrational deactivation pathway through the hydrogen bonds available for excited **A** (**A***) in the complex.

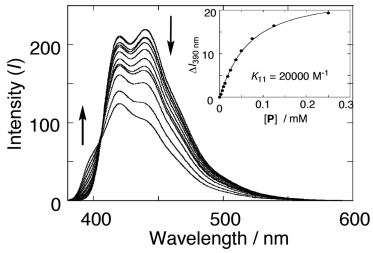

Figure 2. Fluorescence spectral titration of **A** (25 μM) with **P** (0–10 equiv) in CH_2Cl_2 at 25 °C; excitation at 355 nm (one of the isosbestic points upon UV/vis titration; see Figure 1). Inset: Fluorescence intensity changes at 390 nm and the nonlinear least-squares fit assuming the 1:1 stoichiometry.

The fluorescence intensity changes at 390 nm plotted against [**P**] were subjected to the nonlinear least-squares fit, assuming the 1:1 stoichiometry (Figure 2, inset), to give the association constant at 25 °C: $K_{11} = (20 \pm 1) \times 10^3$ M^{-1}. Essentially the same K_{11} value of $(19.0 \pm 0.9) \times 10^3$ M^{-1} was obtained for a more dilute solution of **A** at 5 μM (Figure S5). Similarly, the K_{11} values at 15 and 5 °C were determined (Figure S6) as listed in Table 1. A van't Hoff analysis of the K_{11} values at different

Table 1. Association Constants (K_{11}) for 1:1 Complexation of A with P, P_{NM}, and P_{OM} Determined by Fluorescence Spectral Titration in CH_2Cl_2 at 5, 15, and 25 °C

	$K_{11}/10^3$ M^{-1}		
temperature/°C	**P**	P_{NM}	P_{OM}
25	20 ± 1	35 ± 1	6.4 ± 0.9
15	48 ± 5	100 ± 10	13.0 ± 0.9
5	120 ± 17	250 ± 20	22.0 ± 1.2

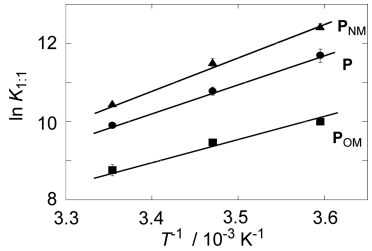

Figure 3. van't Hoff plots of the 1:1 association constants (K_{11}) of **A** with **P**, P_{NM}, and P_{OM} in CH_2Cl_2.

temperatures (Figure 3) allowed us to determine the enthalpy ($\Delta H°$) and entropy ($\Delta S°$) of complexation shown in Table 2. The fluorescence spectral titration experiments with the reference compounds, that is, *N*-methyl-L-prolinol (P_{NM}) and *O*-methyl-L-prolinol (P_{OM}), were also performed at 5, 15, and

Table 2. Thermodynamic Parameters for 1:1 Complexation of A with P, P_{NM}, and P_{OM} in CH_2Cl_2

template	$\Delta G°$/kcal mol^{-1}	$\Delta H°$/kcal mol^{-1}	$T\Delta S°$[a]/kcal mol^{-1}
P	−6.1 ± 0.7	−14.8 ± 0.5	−8.7 ± 0.5
P_{NM}	−6.3 ± 1.5	−16.5 ± 1.0	−10.2 ± 1.0
P_{OM}	−5.1 ± 1.5	−10.2 ± 1.0	−5.1 ± 1.2

[a] T = 298.15 K.

DOI: 10.1021/jacs.6b05598
J. Am. Chem. Soc. 2016, 138, 12187–12201

25 °C to give the K_{11} values shown in Table 1. Analogous van't Hoff plots of these K_{11} values (Figure 3) gave the thermodynamic parameters listed in Table 2; the relevant Job plots and the fluorescence titration results for the complexation of **A** with $\mathbf{P}_{NM}$ and $\mathbf{P}_{OM}$ are shown in Figures S7–S10. It is reasonable that tertiary amine $\mathbf{P}_{NM}$ binds **A** more strongly than secondary amine **P** to afford comparable or slightly more negative $\Delta H°$ (by 1.7 kcal mol^{-1}) and $T\Delta S°$ (by 1.5 kcal mol^{-1} at 25 °C). On the other hand, $\mathbf{P}_{OM}$ turned out to be a much weaker binder as a consequence of the loss of the hydroxyl group, affording less negative $\Delta H°$ (by 4.6 kcal mol^{-1}) and $T\Delta S°$ (by 3.6 kcal mol^{-1}). These results indicate that the hydroxyl group in **P** enhances the affinity to **A** through the enthalpic gain of 4.6 kcal mol^{-1} but has to pay the entropic penalty of 3.6 kcal mol^{-1}, achieving the net free energy gain ($-\Delta G°$) of 1.0 kcal mol^{-1}, and that both the enthalpic gain and the entropic loss caused upon *N*-methylation of **P** are much smaller.

Higher-Order Complexes: CD Spectral Detection and Quantification. As the UV/vis spectral titration (Figure 1) suggested the existence of higher-order complex(es), we closely examined the complexation behavior of **A** with **P** by using CD spectroscopy, a powerful tool for detecting and analyzing higher-order complexation involving two (or more) chromophoric components by observing the exciton coupling behavior at the main band.

The CD spectral Job analysis for elucidating the complex stoichiometry was performed at the same total concentration (0.35 mM) as the UV/vis spectral Job analysis (Figure S1) to reveal a clear exciton couplet at the ^1B_b transition of **A** (Figure 4a), indicating formation of higher-order complex(es) that incorporate at least two **A** molecules. Job plots of the ellipticities at the positive and negative couplet extrema (Figure 4b) revealed peaks not at fraction $x = 0.67$ but at $x = 0.5$ (with significant downward deviations at low and high x values), indicating formation of a *n*:*n* complex ($n \geq 1$). Since 1:1 complex **A**·**P** never produces a CD couplet, the observed couplet is assignable to an unprecedented 2:2 complex $\mathbf{A}_2\cdot\mathbf{P}_2$ (as the simplest one). The unusual bell-shaped Job plot is reasonable, as the concentration of $\mathbf{A}_2\cdot\mathbf{P}_2$ formed is proportional to $[\mathbf{A}]^2$ and $[\mathbf{P}]^2$ and hence discouraged at low [**A**] or [**P**] but enhanced at comparable [**A**] and [**P**]. For the same reason, the formation of $\mathbf{A}_n\cdot\mathbf{P}_n$ ($n \geq 3$) is highly unlikely at submillimolar concentrations. Thus, the complexation equilibrium of **A** with seemingly simple hydrogen-bonding template **P** turned out to be fairly complicated, involving at least 1:1 and 2:2 complexes.

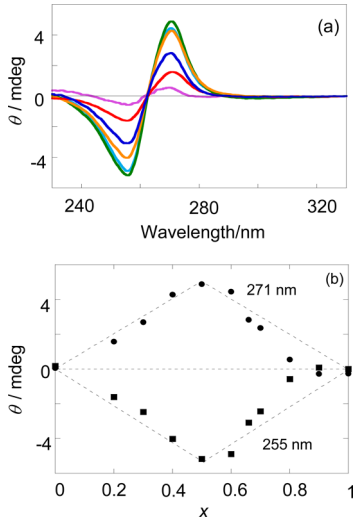

Figure 4. (a) CD spectra of **A** in CH_2Cl_2 in the presence of **P** at various molar fractions (x) of **A**: $x = 0.2$ (red), 0.4 (orange), 0.5 (green), 0.6 (light blue), 0.67 (blue), and 0.8 (purple), where the total concentration of **A** and **P** is fixed at 0.35 mM; measured in a 2 mm cell. (b) Job plots of the ellipticities monitored at the couplet extrema, i.e., 255 and 271 nm.

For more quantitative examination of the complexation equilibria of **A** with **P**, we performed the CD spectral titration experiments with a 0.1 mM solution of **A** in dichloromethane at lower temperatures, where the higher-order complexation is expected to be favored. As exemplified in Figure 5a, the CD

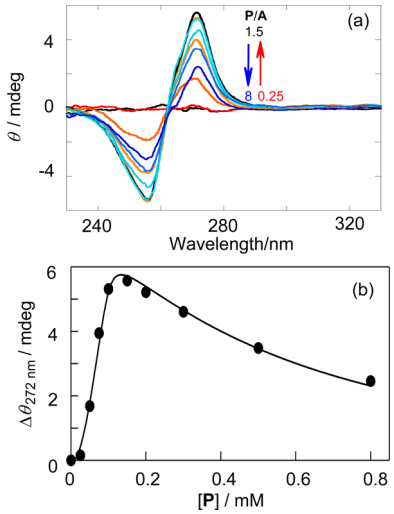

Figure 5. (a) CD spectral titration of **A** (0.1 mM) with **P** (0–0.8 mM) in CH_2Cl_2 at −10 °C. (b) Ellipticity changes monitored at the positive extremum (272 nm) and the result of the nonlinear least-squares fit to the equation derived from the complexation equilibria shown in Scheme 2; for details, see the Experimental Section.

spectra of **A** in the presence of various amounts of **P** obtained at −10 °C showed clear couplets. The couplet intensity at 272 nm rapidly increased with increasing [**P**] up to **P**/**A** = 1 (Figure 5b), indicative of $\mathbf{A}_2\cdot\mathbf{P}_2$ formation, but was not saturated thereafter as anticipated from the equilibrium model that postulates only the 1:1 and 2:2 complexes. Instead, the intensity gradually declined upon further addition of **P** (2–8 equiv) (Figure 5b), which indicates formation of a CD-silent $\mathbf{A}\cdot\mathbf{P}_2$ complex in the presence of excess amounts of **P** by intercepting the 1:1 complex (**A**·**P**). Furthermore, we have shown in a recent work that **A** can form a 2:1 complex with prolinol derivative **T**,[6c] and the enantiodifferentiating photocyclodimerization behavior of **A** mediated by **P** cannot be fully rationalized without postulating a 2:1 complex (vide infra). These facts led us to the somewhat complicated, but complete, higher-order complexation equilibria shown in Scheme 2.

The ellipticity changes upon CD spectral titration (Figure 5b) were fitted to the simulation curve derived from the equilibria shown in Scheme 2 (for details, see the Experimental Section) to obtain the K_{12}, K_{21}, and K_{22} values at each temperature (Figures 5b and S11) by fixing K_{11} at the value extrapolated from those in Table 1. The association constants

DOI: 10.1021/jacs.6b05598
J. Am. Chem. Soc. 2016, 138, 12187–12201

Scheme 2. Complexation Equilibria of A with P

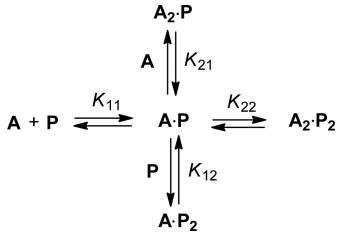

thus obtained at temperatures ranging from 0 to −30 °C are summarized in Table 3, along with those extrapolated to 25 °C.

Table 3. Association Constants for 1:1, 1:2, 2:1, and 2:2 Complexes of A with P in CH_2Cl_2

temperature/°C	K_{11}[a]/10^3 M^{-1}	K_{12}[b]/M^{-1}	K_{21}[b]/M^{-1}	K_{22}[b]/M^{-1}
25	20	390[c]	70[c]	740[c]
0	200[c]	1200± 40	180± 60	2600± 90
−10	550[c]	1800± 250	280± 150	3300± 100
−20	1700[c]	3900± 440	450± 390	6400± 500
−30	5600[c]	5600± 600	740± 580	9800± 700

[a]Experimental or extrapolated K_{11} values from the fluorescence spectral titration at 5−25 °C; see Table 1. [b]Determined by the CD spectral titration (Figures 5 and S10). [c]Extrapolated value.

The association constants in Table 3 reveal that the higher-order complexes, possessing 2−3 (0 °C) or 3−4 orders (−30 °C) of magnitude smaller K values than the 1:1 complex, are undoubtedly minor species in the overall complexation equilibria of **A** with **P**, which are detectable only by examining the CD spectral and photochirogenic (vide infra) behaviors of the chromophoric guest substrates incorporated in the higher-order complexes. Nevertheless, the fact that the carboxylic group in **A** and the β-aminoalcohol moiety in **P** can form these unprecedented ternary and quaternary complexes is crucial, as the hydrogen-bonding partners (i.e., carboxylic acid and β-aminoalcohol) are rather conventional and may be amply found or incorporated in chemical and biological supramolecular systems. Hence, we decided to further elucidate the origin, structures, and properties of the hydrogen-bonding motifs that allow construction of such elaborate complex species.

As shown in Figure 6, the van't Hoff plots of the experimental K_{12}, K_{21}, and K_{22} values shown in Table 3 afforded good straight lines, from the slope and intercept of which the enthalpy and entropy of complexation were calculated for each higher-order complexation, as shown in Table 4. It is reasonable that all of the three higher-order complexations are accompanied by comparable enthalpic gains

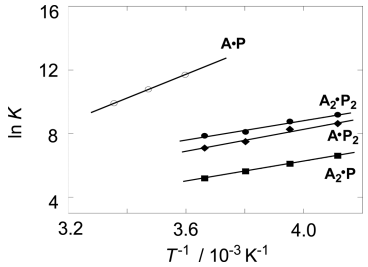

Figure 6. van't Hoff plots for the 1:1, 2:2, 1:2, and 2:1 complexation (from top to bottom); the plot for 1:1 complexation (the same as Figure 4) is included for comparison purposes.

Table 4. Thermodynamic Parameters for Stepwise 1:1, 1:2, 2:1, and 2:2 Complexation of A with P in CH_2Cl_2

A:P	$\Delta G°$/kcal mol^{-1}	$\Delta H°$/kcal mol^{-1}	$T\Delta S°$[a]/kcal mol^{-1}
1:1	−6.1 ± 0.7	−14.8 ± 0.5	−8.7 ± 0.5
1:2	−3.5 ± 1.2	−7.1 ± 0.8	−3.6 ± 0.9
2:1	−2.5 ± 0.1	−6.2 ± 0.1	−3.7 ± 0.1
2:2	−4.0 ± 1.0	−6.1 ± 0.7	−2.1 ± 0.8

[a]T = 298.15 K.

(−ΔH) of 6.1−7.1 kcal mol^{-1} and entropic losses ($T\Delta S$) of 2.1−3.7 kcal mol^{-1} since two relatively weak hydrogen bonds are newly created in each higher-order complex, as elucidated below by the theoretical calculations. It is also interesting that the $\Delta H°-T\Delta S°$ compensation plot of all the thermodynamic parameters obtained in this study (Tables 2 and 4) gives a good straight line (r^2 = 0.970) (Figure S12), suggesting operation of the same binding mechanism (weak noncovalent interactions) despite the apparent difference in stoichiometry; the slope of 0.70 and the intercept of 1.5 kcal mol^{-1} indicate modest conformational changes and minimal desolvation upon complexation, respectively.[11]

The existence of 1:2 complex **A**·$\mathbf{P}_2$ was deduced from the declining CD couplet intensity of $\mathbf{A}_2$·$\mathbf{P}_2$ at higher [**P**] (**P**/**A** ≥ 2) and supported by the equilibrium analysis described above but not directly proven so far. Although the 1:1 complexation of **P** to **A** causes significant changes in the UV/vis spectrum (but no CD signals), the subsequent complexation of another **P** to **A**·**P** affording **A**·$\mathbf{P}_2$ is "invisible" in the UV/vis or CD spectrum. Among the three higher-order complexes, $\mathbf{A}_2$·**P** and $\mathbf{A}_2$·$\mathbf{P}_2$ are expected to undergo rapid intracomplex cyclodimerization upon excitation (vide infra) without emitting light, while **A**·$\mathbf{P}_2$, lacking such a photochemical decay path, is likely to be fluorescent and hence experimentally detectable if its fluorescence lifetime differs from those of **A** and **A**·**P**.

The fluorescence lifetimes (τ) of **A** (5, 25, and 250 μM), excited at the isosbestic point (355 nm) and monitored at λ_{em} = 398 and 440 nm, were measured in the presence of **P** (0−200 equiv) in dichloromethane at 25 °C by using the time-correlated single-photon-counting technique (Figure S13) to give the results shown in Table 5. The population of free **A** and $\mathbf{A}_m$·$\mathbf{P}_n$ complexes (m, n = 1 or 2) at each **P**/**A** ratio was calculated by using the experimental or extrapolated association constants (Tables 1 and 3). At [**A**] = 25 μM and **P**/**A** = 0−200, the contribution of $\mathbf{A}_2$·**P** and $\mathbf{A}_2$·$\mathbf{P}_2$ is negligible (≤1%), and only **A**, **A**·**P**, and **A**·$\mathbf{P}_2$ are to be considered. As can be seen from Table 5, two distinct lifetimes of 14.7 ns (relative abundance A_1 = 0.79) and 6.8 ns (A_2 = 0.21) were detected at **P**/**A** = 1, where only free **A** and **A**·**P** are populated in a 73:27 ratio and therefore the latter lifetime is readily assignable to **A**·**P**. Lifetime measurements at a lower concentration of **A** (5 μM) and **P**/**A** = 0−15, where only free **A** and **A**·**P** exist, gave essentially the same lifetimes of 5.6−6.6 ns for **A**·**P** (Table S2), confirming this assignment. At higher **P**/**A** ratios (≥5), the fluorescence decay became a sum of three exponential functions to give a short lifetime of 2.5−3.3 ns in addition to the known lifetimes of 15 ns for free **A** and 6.0−6.5 ns for **A**·**P**. This new species is assignable to **A**·$\mathbf{P}_2$ on the basis of the parallel behavior of the A_3 value (at both λ_{em}) and the population of **A**·$\mathbf{P}_2$. Comparison of the relative abundance of

DOI: 10.1021/jacs.6b05598
J. Am. Chem. Soc. 2016, 138, 12187−12201

Table 5. Population of Free A and 1:1, 1:2, 2:1, and 2:2 Complexes in the Ground State and Fluorescence Lifetimes of A (τ_1), A·P (τ_2), and A·P_2 (τ_3) in CH_2Cl_2[a]

		population/%[b]												
[A]/μM	P/A	A	A·P	A·P_2	A_2·P	A_2·P_2	λ_{em}	τ_1/ns	A_1	τ_2/ns	A_2	τ_3/ns	A_3	χ^2
25	0	100					440	15.0						1.1
	1	73	27				440	14.7	0.79	6.8	0.21			1.1
	5	31	65	3		1	398	15.0[c]	0.04	6.3	0.68	2.9	0.28	1.1
							440	15.0[c]	0.45	6.3	0.47	3.3	0.08	1.1
	50	3	65	31		1	398	15.0[c]	0.02	6.0	0.62	2.5	0.36	1.1
							440	15.0[c]	0.11	6.3	0.75	2.8	0.14	1.1
	200		34	66			398	15.0[c]	0.00	6.3	0.44	2.8	0.56	1.0
							440	15.0[c]	0.03	6.5	0.53	2.7	0.44	1.1
250	1	35	56	2		7	398	15.0[c]	0.05	6.3[c]	0.40	2.8	0.55	1.1
							440	15.0[c]	0.36	6.8	0.43	2.1	0.21	1.1
	2	13	69	8		10	398	15.0[c]	0.03	6.3[c]	0.27	3.1	0.70	1.1
							440	15.0[c]	0.15	6.3[c]	0.49	2.4	0.36	1.1

[a]Measured with a 25 μM solution of **A** in aerated CH_2Cl_2 at 25 °C; excitation wavelength = 355 nm (the isosbestic point observed upon UV/vis titration); excitation and emission slits = 10 nm. [b]Calculated by using the association constants shown in Table 3; values <1% not shown. [c]Deconvolution performed with fixed τ_1 and/or τ_2.

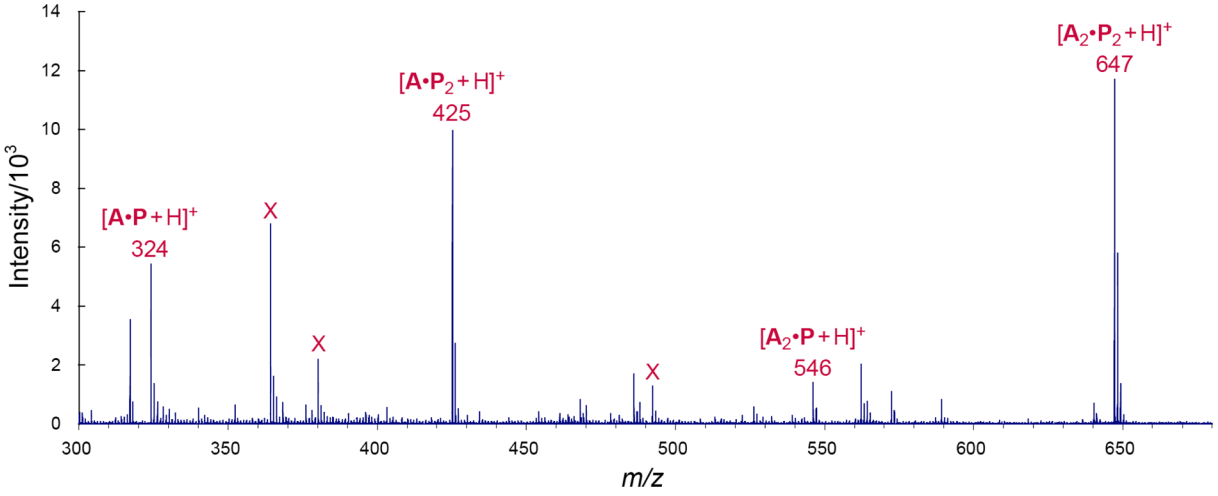

Figure 7. Cold-spray ionization mass spectrum (part) of a 1:9 acetonitrile/dichloromethane solution containing 0.25 mM **A** and 0.25 mM **P**; among the unidentified minor peaks, the ones marked by X are assignable to the impurities contained in **P** that were used; spray temperature = −25 °C; see Figure S14 for the full-range spectrum.

each species (the $A_1/A_2/A_3$ ratio) obtained at λ_{em} = 398 and 440 nm reveals progressive hypsochromic shifts of the fluorescence upon stepwise complexation of **A** with **P**. No additional fluorescent species, such as A_2·**P** and A_2·P_2, was detected, and essentially the same τ_1, τ_2, and τ_3 values (with smaller A_1 and larger A_2 and A_3 values) were obtained under the photoreaction conditions ([**A**] = 0.25 mM), indicating that singlet-excited A_2·P_2 (7−10% population at **P**/**A** = 1−2) is not fluorescent and more crucially that ground-state **A**, **A**·**P**, and **A**·P_2 species cannot dynamically quench any of the excited **A** species, and therefore, the cyclodimers are produced only from the intracomplex photoreactions in A_2·**P** and A_2·P_2.

Direct Observation of Higher-Order Complexes by CSI-MS. The existence of higher-order complexes was further examined by using cold-spray ionization mass spectrometry (CSI-MS)[12] to obtain direct evidence. Thus, a sample solution of **A** (0.25 mM) and **P** (0.25 mM) in dichloromethane, containing 10% acetonitrile for facilitating ionization, was subjected to the CSI-MS analysis to reveal the peaks at *m*/*z* 324, 425, 546, and 647 (Figures 7 and S14), which correspond to the nominal molecular weights of the protonated forms of **A**·**P**, **A**·P_2, A_2·**P**, and A_2·P_2 complexes, respectively. The relative intensities of these peaks (**A**·**P**/**A**·P_2/A_2·**P**/A_2·P_2 = 1:1.83:0.26:2.15) do not agree with the population of these species in dichloromethane at −25 °C: **A**·**P**/**A**·P_2/A_2·**P**/A_2·P_2 = 1:0.021:0.0031:0.74 (Table 7, run 17) with the higher-order complexes (**A**·P_2, A_2·**P**, and A_2·P_2) being consistently emphasized in CSI-MS. For this disagreement, the addition of 10% acetonitrile that would cause equilibrium shifts and the difference in ionization efficiency of each species are likely to be jointly responsible, while the general emphasis of the higher-order complexes would arise from the sample concentration by solvent evaporation upon cold-spraying, although the stronger emphasis of **A**·P_2 and A_2·**P** than A_2·P_2 is not readily rationalized at the moment.

Structure Elucidation for Higher-Order Complexes. To better understand the structural aspects of higher-order complexes revealed in the spectroscopic studies, we first experimentally defined the necessary conditions for constructing the higher-order, in particular 2:2, complexes between **A** and **P** by examining the complexation behavior of partially "impaired" prolinol templates, that is, *N*-methyl (P_{NM}) and *O*-

DOI: 10.1021/jacs.6b05598
J. Am. Chem. Soc. 2016, 138, 12187−12201

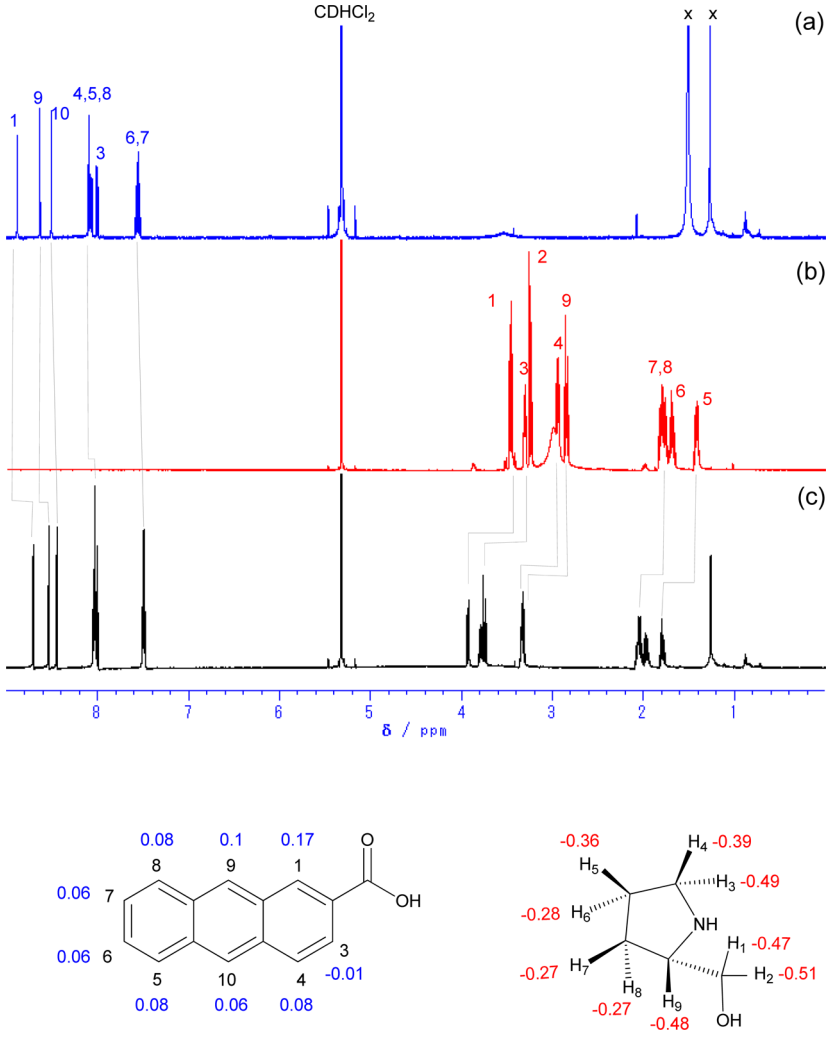

Figure 8. Top: ^{1}H NMR spectra (600 MHz) of (a) **A** (1 mM), (b) **P** (5 mM), and (c) a 1:1 mixture of **A** and **P** (5 mM each) measured in CD_2Cl_2 at room temperature (ca. 25 °C) or at 30 °C (only for (a), due to the low solubility of **A**); the population of each species is calculated as 9% **A**, 39% **A**·**P**, 3% **A**·$\mathbf{P}_2$, 1% $\mathbf{A}_2$·**P**, and 48% $\mathbf{A}_2$·$\mathbf{P}_2$ by using the *K* values in CH_2Cl_2 at 25 °C (Table 3). Bottom: Upfield and downfield shifts in ppm (shown as positive and negative values, respectively) of **A** and **P** protons caused upon complexation.

methyl ($\mathbf{P}_{OM}$) derivatives, by CD spectroscopy. As shown in Figures S15 and S16, $\mathbf{P}_{NM}$ and $\mathbf{P}_{OM}$ caused significant changes in UV/vis spectra, as was the case with **P**, but never induced CD signals over the entire absorption range of **A**, unequivocally revealing the absence of a 2:1 or 2:2 complex in the solution. This result indicates that both the amino and hydroxyl protons in **P** are indispensable for constructing the higher-order complexes. It is also crucial that **T** (TKS159), lacking the amino proton, still affords a stable 1:1 complex with **A** by forming a nine-membered hydrogen-bonding network and a less stable 2:1 complex with additional **A**.[6] Another important fact to be taken into account is the exclusive formation of the head-to-head cyclodimers upon photocyclodimerization in the presence of **P** at low temperatures, details of which will be discussed in the later sections (Table 7). Also, the NMR spectral examination of a CD_2Cl_2 solution of **A** (5 mM) in the presence of **P** (5 mM) at 25 °C showed the upfield shifts of **A** protons by up to 0.17 ppm and the downfield shifts of **P** protons by up to 0.51 ppm (Figure 8), which are attributable to the $\pi-\pi$ stacking and the protonation to the amino nitrogen, respectively.

Taking into account all the available experimental results obtained above, we constructed two plausible structures for the 2:2 complex, the first of which was derived by straightforwardly connecting two 1:1 complexes with dual hydrogen bonds between the amino proton of **P** and the carbonyl oxygen of facing **A** and hence is called the "parallel-link" model; for the structures, see Figure S17. The second one called the "cross-link" model was constructed by switching the hydrogen-bonding partner upon interaction with another 1:1 complex to make two **A**s being doubly bridged by two **P**s, which in turn were linked together with two N–H···O hydrogen bonds; see Figure 9. Both the models allow for the existence of four diastereomeric conformers, in which the enantiotopic faces of two **A**s are confronting in *re-re*, *re-si*, *si-re*, and *si-si* manner, as illustrated in Figures 9 and S17. All of the conformers were geometry-optimized by the dispersion-corrected DFT method at the DFT-D3-B-LYP/def2-TZVP level[13] incorporating the COSMO solvation model.[14] The energy of each optimized structure was calculated by the SCS-MP2 method[15] using a basis set of def2-TZVPP quality to give the relative stability and population for the cross- and parallel-link models (Tables S3–S5). As can be seen from Table S3, all of the parallel-linked

DOI: 10.1021/jacs.6b05598
J. Am. Chem. Soc. 2016, 138, 12187–12201

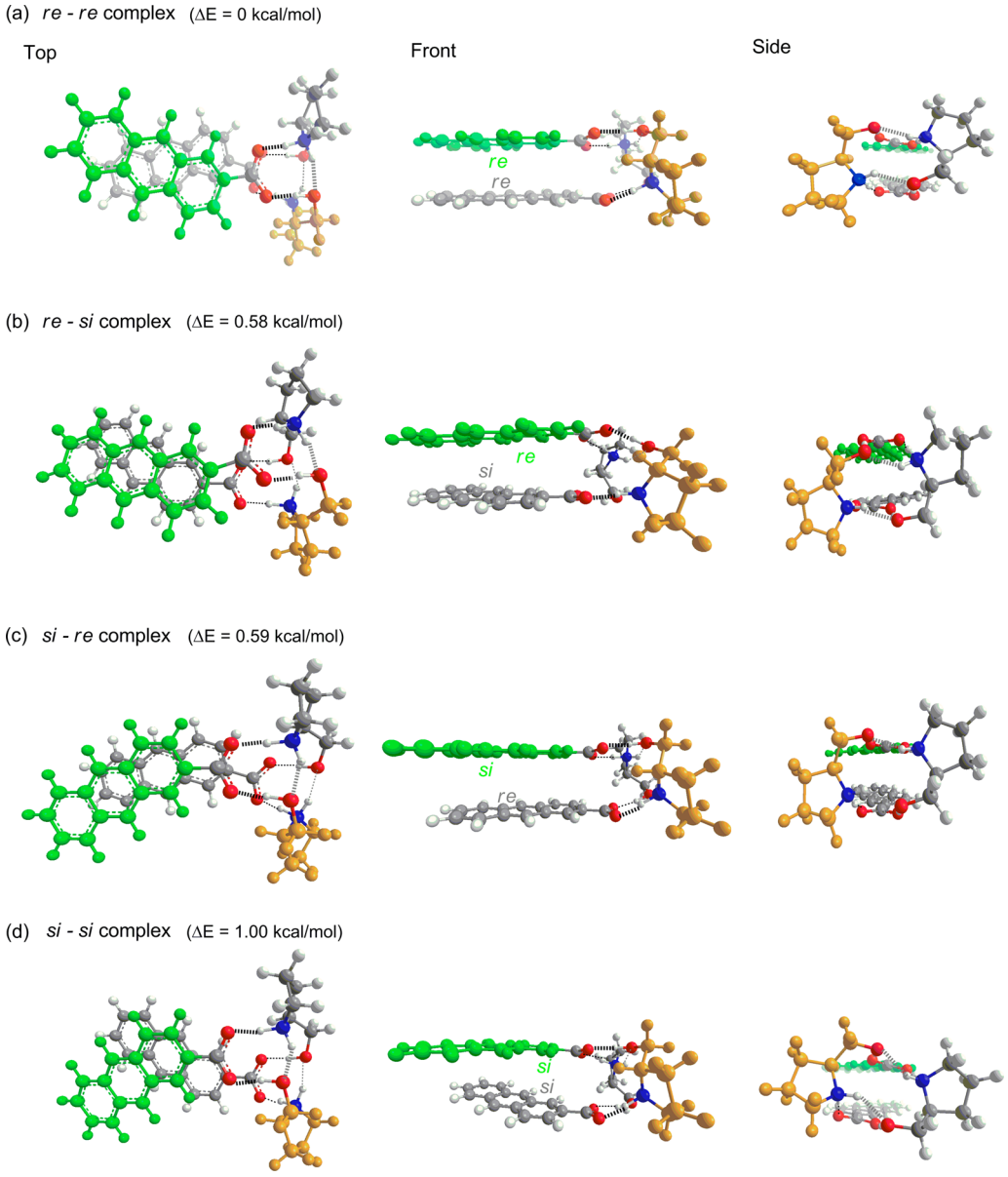

Figure 9. Structures of (a) *re-re*, (b) *re-si*, (c) *si-re*, and (d) *si-si* conformers of the cross-linked model of $\mathbf{A}_2{\cdot}\mathbf{P}_2$ geometry-optimized at the DFT-D3-B-LYP/def2-TZVP level (with the COSMO solvation model), while the relative energies of the four conformers were calculated at the SCS-MP2/def2-TZVPP level including the COSMO solvation model.

conformers are higher in energy by 1.1−2.5 kcal mol^{-1} than the most stable cross-linked *re-re* conformer and hence will not be considered further. In contrast, the cross-linked conformers are more stable to give the relative population shown in Table 6. Note, however, that all the cross-linked conformers possess very shallow potential energy curves against the torsion angle between the anthracene and carboxyl planes of the complexes (Figure S18), allowing wide angular variations at ambient temperatures.

Table 6. Relative Energies (Δ*E*) Calculated at the SCS-MP2/def2-TZVPP Level Using the COSMO Solvation Model and Boltzmann Distribution at 25 °C of Four Conformers of a "Cross-Linked" 2:2 Complex[a]

	re-re	*re-si*	*si-re*	*si-si*
Δ*E*/kcal mol^{-1}	≡0	+0.58	+0.59	+1.00
population/%	51.7	19.5	19.2	9.6

[a]Geometries were optimized at the DFT-D3-B-LYP/def2-TZVP level using the COSMO solvation model.

In our previous studies on the theoretical simulation of experimental CD spectra[9a] and the X-ray crystallographic structure of enantiopure cyclodimer **3**_,[9b] we unequivocally correlated the enantiotopic faces of two cyclodimerizing **A**s with the absolute configuration of the cyclodimer derived therefrom. In the present case, the HH-oriented *re-re* and *si-si* conformers afford **3**_ and **3**$_+$, respectively, while the *re-si* and *si-re* conformers give achiral **4**. As can be seen from Table 6, the stability order of the four conformers and their populations at 25 °C are *re-re* (51.7%) > *re-si* (19.5%) ≈ *si-re* (19.2%) > *si-si* (9.6%), predicting preferential formation of **3**_ in 69% ee (provided that each conformer cyclodimerizes at the same rate upon irradiation). This prediction was experimentally verified indeed, but the actual ee values obtained were appreciably

DOI: 10.1021/jacs.6b05598
J. Am. Chem. Soc. 2016, 138, 12187−12201

Table 7. Population of Free 2-Anthracenecarboxylic Acid (A) and Its 1:1, 1:2, 2:1, and 2:2 Complexes with L-Prolinol (P) in the Ground State and Results of Enantiodifferentiating Photocyclodimerization of A Mediated by P and Its *N*- and *O*-Methyl Derivatives (P_{NM} and P_{OM})[a]

				population/%[c]								relative yield/% (ee/%)[d]					
run	template	temp/°C	P/A	free A	A·P	A·P_2	A_2·P	A_2·P_2	A_2·P_2/A_2·P	irradiation time/min	conv/% (rel. rate)[b]	1	2	3	4	% HH[e]	4/3
1	none	25	0	100						30	50	33	22 (0)	24 (0)	21	45	0.9
2		0	0	100						3	7(≡1)	36	21 (2)	27 (0)	16	43	0.6
2a										30	32	36	20 (0)	28 (0)	16	44	0.6
3		−25	0	100						120	12[f]	41	15 (−3)	34 (0)	10	44	0.3
4	P_{NM}	25	5	3	97					30	61	35	23 (2)	24 (3)	18	42	0.8
5		−25	5	0	100					30	43	36	26 (0)	22 (−2)	16	38	0.7
6	P_{OM}	25	10	6	94					30	78	22	15 (1)	28 (−1)	35	63	1.3
7		−25	10	0	100					30	39	25	15 (2)	25 (2)	35	60	1.4
8	P	0	0.1	91	8.6	0.005	0.3	0.5	1.4	3.5	9 (1.1)	15	9 (1)	36 (−1)	40	76	1.1
9			0.25	77	20	0.03	0.7	2.4	3.7	2	10 (2.1)	9	5 (3)	36 (−5)	50	86	1.4
10			0.5	55	36	0.1	0.8	7.8	9.5	1	9 (3.7)	5	3 (2)	35 (−17)	57	92	1.6
11			1	13	64	1.8	0.3	21	69	0.83	9 (4.6)	3	2 (*g*)	28 (−39)	67	95	2.4
11a										30	83	2	2 (*g*)	35 (−21)	61	96	1.7
12			2	1.4	62	16	0.03	21	630	0.75	7 (4.2)	2	1 (*g*)	29 (−42)	68	97	2.3
12a										30	92	1	1 (*g*)	30 (−41)	68	98	2.3
13			5	0.2	43	46	0.004	11	2600	1.33	8 (2.6)	1	1 (*g*)	28 (−43)	70	98	2.5
13a										30	87	1	1 (*g*)	30 (−42)	68	98	2.3
14			10	0.1	27	68	0.001	4.6	6000	2.5	10 (1.7)	1	1 (*g*)	30 (−42)	68	98	2.3
14a										30	95	1	1 (*g*)	29 (−35)	69	98	2.4
15		−25	0.5	56	29	0.02	1.8	13	6.8	0.83	11 (5.9)	4	2 (*g*)	38 (−16)	56	94	1.5
16			0.85	20	47	0.2	1.0	32	32	0.7	12 (6.7)	3	1 (*g*)	33 (−32)	63	96	1.9
17			1	3.7	55	1.2	0.2	40	200	0.5	11 (8.9)	1	1 (*g*)	28 (−50)	70	98	2.5
18			2	0.1	41	34	0.003	25	7300	0.5	8 (7.6)	1	1 (*g*)	27 (−50)	71	98	2.6
19		−50	0.85	20	30	0.01	2.4	47	19	0.8	8 (3.9)	4	2 (*g*)	36 (−36)	58	94	1.6
20			1	0.7	36	0.5	0.1	63	640	0.5	6 (5.1)	3	1 (*g*)	30 (−54)	66	96	2.2
21			2	0.002	19	58	2×10^{-4}	23	1.5×10^{5}	1.0	11 (4.6)	1	0 (*g*)	32 (−58)	67	99	2.1
22		−80[h]	1	0.1	23	0.1	0.03	77	2900	2.5	9 (1.4)	2	1 (*g*)	42 (−63)	55	97	1.3
23			2	3×10^{-5}	8.4	77	2×10^{-6}	15	6.3×10^{6}	1.8	7 (1.6)	2	1 (*g*)	42 (−65)	55	97	1.3
24		−90[i]	5	$<1 \times 10^{-8}$	25	46	$<1 \times 10^{-8}$	29		6.0	*j*	2	0	44 (−68)	54	98	1.2
25		−95[i]	5	$<1 \times 10^{-8}$	19	54	$<1 \times 10^{-8}$	27		6.0	*j*	0	0	51 (−72)	49	100	0.96

[a]Irradiation of **A** (0.25 mM, unless noted otherwise) performed in CH_2Cl_2 at $\lambda > 320$ nm in the presence and absence of prolinol derivative (**P**, P_{NM}, or P_{OM}) under N_2. [b]Consumption of **A** determined by monitoring the UV/vis spectral change at 390 nm and the relative rate compared with the photocyclodimerization of free **A** at 25 °C, estimated by dividing the conversion by the irradiation time (calculated only for low-conversion runs to estimate the initial rate). [c]Population of free **A** and **A**·**P** complexes calculated by extrapolating the association constants shown in Tables 1 and 3. [d]The negative sign for the ee value indicates preferred formation of (*P*)-**3** (**3**_); [9] error in yield = ±1%; error in ee = ±3%. [e]HH = (**3** + **4**)/(**1** + **2** + **3** + **4**). [f]Conversion not comparable with the other data due to the partial precipitation of **A** at −25 °C in the absence of **P**. [g]Not determined due to low chemical yield. [h][**A**] = 0.1 mM. [i][**A**] = 0.01 mM due to low solubility. [j]Not determined.

J. Am. Chem. Soc. 2016, 138, 12187−12201
DOI: 10.1021/jacs.6b05598

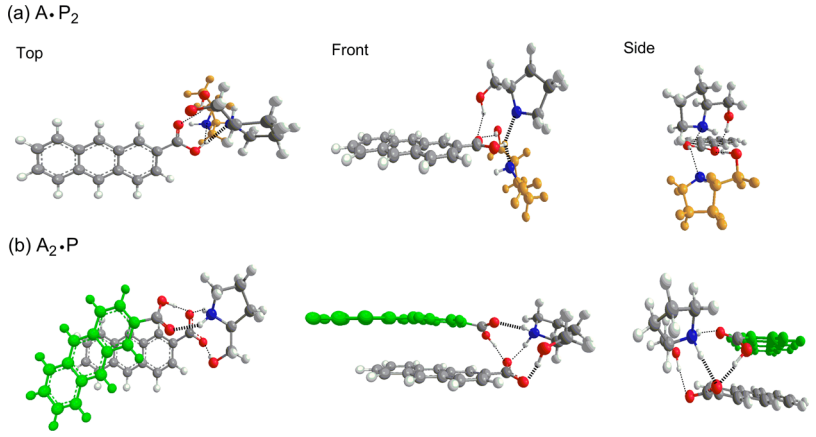

Figure 10. Structures of (a) **A**·$\mathbf{P}_2$ and (b) *si-si* conformer of $\mathbf{A}_2$·**P** complex optimized at the DFT-D3-B-LYP/def2-TZVP level.

lower (43% ee) (Table 7), implying some overestimation of the relative energy by the SCS-MP2 method.

The structures of **A**·$\mathbf{P}_2$ and $\mathbf{A}_2$·**P** were also optimized at the same level of theory. The initial structures were generated by placing an extra **P** or **A** in the vicinity of the 1:1 complex to maximize the number of hydrogen bonds to be formed, without losing the original ones; the optimized structures thus obtained are illustrated in Figure 10 (see also Tables S7 and S8).

In 1:2 complex **A**·$\mathbf{P}_2$ (Figure 10a), the second **P** is bonded to **A** of the original 1:1 complex through two hydrogen bonds linking the carboxyl proton and the nitrogen, as well as the carbonyl oxygen and the hydroxyl proton. These additional hydrogen bonds accelerate the vibrational deactivation of **A***, leading to the much shorter fluorescence lifetime for **A**·$\mathbf{P}_2$ (3 ns) than for free **A** (15 ns) or **A**·**P** (6 ns) (Table 5). From the stereochemical point of view, only poor or even negligible enantiotopic face selectivity is anticipated for the photocyclodimerization through **A**·$\mathbf{P}_2$, as neither the *re* nor *si* face of **A** is shielded by **P**. In the case of $\mathbf{A}_2$·**P** (Figure 10b), two new hydrogen bonds are formed between the carboxyl proton of the second **A** and the carbonyl oxygen of the original **A**·**P** and also between the carbonyl oxygen of the second **A** and the ammonium proton. This structure shares the same hydrogen-bonding motif with the 2:1 complex of **A** with **T** (TKS) reported previously.[6c]

Enantiodifferentiating Photocyclodimerization of 2-Anthracenecarboxylic Acid Mediated by Chiral Hydrogen-Bonding Templates. Photoreaction of **A** (0.25 mM) was performed at $\lambda > 320$ nm in the presence and absence of prolinol template (**P**, $\mathbf{P}_{NM}$, or $\mathbf{P}_{OM}$) in dichloromethane at temperatures ranging from +25 to −25 °C or to −80 °C. In most cases, short and long irradiation periods, typically 0.5−3 min and 30−120 min, were employed to know the initial product distribution and ee (at conversion <10%) and their subsequent changes upon prolonged irradiation. The irradiated samples were analyzed by reverse-phase chiral HPLC on a tandem ODS + OJ-RH column. Table 7 summarizes the results of photocyclodimerization, as well as the population of free **A** and **A**·**P**, **A**·$\mathbf{P}_2$, $\mathbf{A}_2$·**P**, and $\mathbf{A}_2$·$\mathbf{P}_2$ complexes calculated by using the (extrapolated) association constants K_{mn} (m, n = 1 or 2) under the photoreaction conditions employed.

Photocyclodimerization Mediated by *N*- or *O*-Methylated L-Prolinol. Photoirradiation of **A** in the absence of template afforded *anti*- and *syn*-HT dimers (**1** and **2**) and *anti*- and *syn*-HH dimers (**3** and **4**) almost randomly at 25 °C (Table 7, run 1) as reported earlier,[6a] but with appreciably higher preference for *anti*-isomers **1** and **3** at lower temperatures (runs 2 and 3), while % HH was kept constant at 43−45% and the (**1** + **4**)/(**2** + **3**) ratio at near unity, suggesting a perpendicular approach of reacting **A*** and **A** and subsequent rotations of both components to the opposite directions in nearly equal probabilities.[6b] Irradiation of **A** in the presence of reference template $\mathbf{P}_{NM}$ (5 equiv) at both 25 and −25 °C, where essentially only 1:1 complex **A**·$\mathbf{P}_{NM}$ exists, gave racemic **2** and **3** and product distributions very similar to that observed for free **A** at 25 °C (compare run 1 with runs 4 and 5), indicating negligible effect of complexation with $\mathbf{P}_{NM}$.

In contrast, the complexation with $\mathbf{P}_{OM}$ led to somewhat different photocyclodimerization behaviors (runs 6 and 7), that is, appreciably larger conversion and higher preference for HH dimers (HH = 60−63% versus 43−45% for free **A**), in particular, for sterically most congested *syn*-HH dimer **4** (**4**/**3** = 1.3−1.4 versus 0.3−0.9 for free **A**), irrespective of the irradiation temperature. These results would be accounted for by assuming some additional pathway or complex species leading specifically to *syn*-HH dimer **4** at the expense of HT dimers **1** and **2**. Since CD spectral inspections revealed no detectable signals in the main band (Figure S14b), we would suggest the following possibilities: (1) the formation of a weak 2:2 complex $\mathbf{A}_2$·$(\mathbf{P}_{OM})_2$, which is too low in concentration to be detected spectroscopically but sufficient to give the HH dimers in detectable yields upon irradiation; or (2) the HH stacking interaction of two **A**·$\mathbf{P}_{OM}$ complexes facilitated not in the ground but in the excited state during the course of photocyclodimerization. Although the former mechanism seemed more plausible in view of the % HH value (60−63%) independent of the temperature as well as the enhanced production of *syn*-HH **4** observed for $\mathbf{A}_2$·$\mathbf{P}_2$ (runs 11−14 and 17−25), no further examinations were made due to the lack of experimental tools for analyzing such a low-concentration species.

Photocyclodimerization Mediated by L-Prolinol. Addition of **P** caused dramatic changes in photocyclodimerization rate, yield, and enantioselectivity. As shown in Table 7 (runs 11−14), the photocyclodimerization of **A** in the presence of **P** (1−10 equiv) at 0 °C was accelerated by a factor of 1.7−4.6 in apparent rate, relative to free **A** (run 2), to afford the HH dimers in 95−98% selectivity and **3**_ in 39−43% ee. The preferential formation of **3**_ with *P*-absolute configuration[9] agrees with the favored *re-re* conformer in $\mathbf{A}_2$·$\mathbf{P}_2$ (Figure 9).

DOI: 10.1021/jacs.6b05598
J. Am. Chem. Soc. 2016, 138, 12187−12201

The rate enhancement, the exclusive formation of HH dimers, and the steady HH selectivity and ee value observed at **P**/**A** ≥ 1 are reasonably accounted for in terms of the intracomplex photocyclodimerization of $\mathbf{A}_2\cdot\mathbf{P}_2$. These results also reveal that the intermolecular photocyclodimerization is much slower for free **A**, **A**·**P**, and $\mathbf{A}\cdot\mathbf{P}_2$ at this concentration, despite their relatively high populations of up to 13, 63, and 68%, respectively, compared to that of $\mathbf{A}_2\cdot\mathbf{P}_2$ (5−21%).

Intriguingly, the ee of **3** rapidly faded out from 39 to 1% by reducing the **P**/**A** ratio from 1 to 0.1 (runs 8−11) or upon prolonged irradiation at **P**/**A** = 1 (run 11a), while the HH selectivity and the rate were still kept higher than those for free **A** (runs 2 and 2a) even at **P**/**A** = 0.1, indicating the existence of an additional less enantioselective rapid route to the HH dimers at **P**/**A** < 1 in addition to the competition for **P** with the HH dimers produced upon prolonged irradiation. As can be seen from the population of complex species in Table 7 (runs 8−11), reducing the **P**/**A** ratio from 1 to 0.1 leads to a rapidly growing population of free **A** (from 13 to 91%) at substantial losses of **A**·**P** (from 63 to 8.6%) and $\mathbf{A}_2\cdot\mathbf{P}_2$ (from 21 to 0.5%). Crucially, the population of $\mathbf{A}_2\cdot\mathbf{P}$ is not greatly affected but rather kept constant at 0.3−0.8% over the **P**/**A** ratios of 0.1−1, leading to a sharp decrease of the $\mathbf{A}_2\cdot\mathbf{P}_2/\mathbf{A}_2\cdot\mathbf{P}$ ratio from 69 to 1.4. Hence, the rapidly declining ee (from 39 to 1%) and the slowly declining HH selectivity (from 95 to 76%) observed at **P**/**A** < 1 are rationalized by assuming that $\mathbf{A}_2\cdot\mathbf{P}_2$ is the only source of the significant enantioselectivity, while $\mathbf{A}_2\cdot\mathbf{P}$ affords exclusively the HH dimers with negligible enantioselectivity at a much faster rate than $\mathbf{A}_2\cdot\mathbf{P}_2$. The relative photocyclodimerization rate is estimated as ca. 10 from the relative abundance ($\mathbf{A}_2\cdot\mathbf{P}_2/\mathbf{A}_2\cdot\mathbf{P}$ = 9.5) and the nearly half-reduced ee of **3** at **P**/**A** = 0.5 (runs 10 and 11). The *syn*/*anti* selectivity (**4**/**3** ratio) upon photocyclodimerization of $\mathbf{A}_2\cdot\mathbf{P}$ is estimated as 1.3 by subtracting the contribution of HH dimers derived from free **A** (91% population) from the product distribution observed at **P**/**A** = 0.1 (run 8), while that for $\mathbf{A}_2\cdot\mathbf{P}_2$ is readily calculated as 2.4 by averaging the **4**/**3** ratios at **P**/**A** = 1−10 (runs 11−14).

At **P**/**A** ≥ 2, the HH dimers were produced almost exclusively (in ≥97% combined yield) and the ee of **3** was kept constant at 42%, indicating that the intracomplex photocyclodimerization of $\mathbf{A}_2\cdot\mathbf{P}_2$ is much faster than the intermolecular photocyclodimerization of **A**, **A**·**P**, and $\mathbf{A}\cdot\mathbf{P}_2$. From the comparison of the conversion at **P**/**A** = 2 (run 12) versus that at **P**/**A** = 0 (run 2), we can estimate the relative photocyclodimerization rate of $\mathbf{A}_2\cdot\mathbf{P}_2$ against free **A** as ca. 20 (thus, the rate increases in the order **A** (≡1) < $\mathbf{A}_2\cdot\mathbf{P}_2$ (20) < $\mathbf{A}_2\cdot\mathbf{P}$ (200)) under the conditions employed; note, however, that the comparison is made between the intracomplex versus intermolecular photocyclodimerization and hence is concentration-dependent. An important conclusion derived from the above examinations is that $\mathbf{A}_2\cdot\mathbf{P}_2$ and, in particular, $\mathbf{A}_2\cdot\mathbf{P}$ are very minor species in quantity in the **A**−**P** equilibria but dominate the photocyclodimerization behavior including the stereochemical outcomes. It is also crucial from the synthetic viewpoint that, as far as an excess amount of template is present (**P**/**A** ≥ 2), the initial ee of 42% can be maintained up to 87−95% conversion upon prolonged irradiation (runs 12a−14a).

Temperature Effects. Photocyclodimerization of **A** in the presence of **P** (0.5−2 equiv) at −25 °C afforded the HH dimers in 94−98% combined yield (runs 15−18) and **3**_ in 50% ee at **P**/**A** ≥ 1 (runs 17 and 18). The photocyclodimerization of $\mathbf{A}_2\cdot\mathbf{P}_2$ (runs 17 and 18) was accelerated by a factor of ca. 15 when compared with that of $\mathbf{A}\cdot\mathbf{P}_{NM}$ (run 5), which was used as a reference substrate due to the low solubility of **A** at −25 °C (see footnote *f* for run 3 in Table 7). The relative abundance of 2:2 and 2:1 complexes ($\mathbf{A}_2\cdot\mathbf{P}_2/\mathbf{A}_2\cdot\mathbf{P}$ = 32) and the reduction of ee from 50 to 32% at **P**/**A** = 0.85 (run 16) enabled us to estimate the relative photocyclodimerization rate of $\mathbf{A}_2\cdot\mathbf{P}$ versus $\mathbf{A}_2\cdot\mathbf{P}_2$ as 13, which is comparable to the value (15) obtained by using the relevant values at **P**/**A** = 0.5 (run 15). The consistently faster intracomplex photocyclodimerization of $\mathbf{A}_2\cdot\mathbf{P}$ versus $\mathbf{A}_2\cdot\mathbf{P}_2$ at both 0 and −25 °C is attributable to the conformationally less restricted structure of the former complex (compare Figure 10b with Figure 9a).

Upon irradiation at temperatures ≤−25 °C, where $\mathbf{A}_2\cdot\mathbf{P}_2$ becomes the dominant fast photocyclodimerizing species ($\mathbf{A}_2\cdot\mathbf{P}_2 \gg \mathbf{A}_2\cdot\mathbf{P}$) at **P**/**A** ≥ 1, the HH selectivity was kept high at 96−99% and the chemical and optical yields of **3** were gradually enhanced to reach 51% yield and 72% ee at −95 °C (run 25). Note that these HH selectivities (of up to 99%) and ee values (of up to 72%) are much higher than those obtained for the same photoreaction mediated by more elaborate confining hosts designed for better HH selectivity, such as 6^A,6^C-diamino- and 6-(2-aminoethyl)amino-γ-cyclodextrins, which afford 42% HH and 27% ee and 74% HH and 41% ee, respectively.[16]

The high preferences for HH dimers and **3**_ upon photocyclodimerization of **A** mediated by **P** are consistent with the stability order of the $\mathbf{A}_2\cdot\mathbf{P}_2$ conformers evaluated by the theoretical calculations: *re-re* > *re-si* ≈ *si-re* > *si-si* (Figure 9 and Table 6). Thus, the most abundant *re-re* conformer affords **3**_ with *P* configuration as the major enantiomer, while the *re-si* and *si-re* conformers photocyclodimerize to achiral **4** and the least stable *si-si* conformer to **3**$_+$. To better understand the origin of the observed selectivities, the *P*/*M* enantiomer (**3**_/**3**$_+$) and *syn*/*anti* (**4**/**3**) ratios obtained at various temperatures were subjected to Eyring analyses. The logarithms of **3**_/**3**$_+$ and **4**/**3** ratios were plotted against the inverse temperature to give good regression lines (Figure 11), from the slopes and

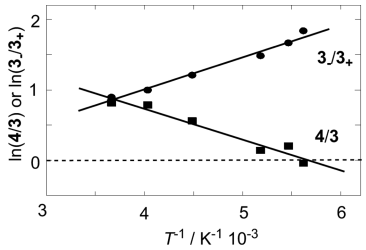

Figure 11. Eyring plots of the *syn*/*anti* ratio (**4**/**3**) and the enantiomer ratio (**3**_/**3**$_+$); see Table 7 for the original data.

intercepts of which the differential activation parameters for the enantio- and *syn*/*anti* selectivities upon photocyclodimerization via $\mathbf{A}_2\cdot\mathbf{P}_2$ were calculated as listed in Table 8. It is

Table 8. Differential Activation Parameters for the *syn*/*anti* (4/3) and Enantio (3_/3$_+$) Selectivities upon Enantiodifferentiating Photocyclodimerization via a 2:2 $\mathbf{A}_2\cdot\mathbf{P}_2$ Complex in CH_2Cl_2

selectivity	$\Delta\Delta G$/ kcal mol^{-1}	$\Delta\Delta H$/ kcal mol^{-1}	$T\Delta\Delta S^a$/ kcal mol^{-1}
syn/*anti* (**4**/**3**)	0.60 ± 0.17	0.87 ± 0.10	1.47 ± 0.14
enantio (**3**_/**3**$_+$ or *P*/*M*)	0.41 ± 0.12	0.92 ± 0.07	0.51 ± 0.10

[a] T = 298 K.

DOI: 10.1021/jacs.6b05598
J. Am. Chem. Soc. 2016, 138, 12187−12201

Table 9. Enantiodifferentiating Photocyclodimerization of A (0.25 mM) Mediated by L- and D-P Mixtures (0.5 mM in Total) in Ratios Ranging from 100:0 (100% ee) to 25:75 (−50% ee) in CH_2Cl_2 at −50 °C[a]

			yield/%					
ee_{cat}/%	irradiation time/min	conv/%	1	2	3	4	ee_{prod}(3)/%	ee_{prod}/ee_{max}[b]
100	1.5	12	1	0	34	65	−57	100
75	2	8	2	1	33	64	−48	84
50	1.5	7	1	1	33	65	−36	63
25	1.5	6	2	1	32	65	−19	33
−50	1.5	6	1	1	33	65	34	−60

[a]For the detailed conditions, see the footnotes of Table 7. [b]The normalized ee value in %, where the ee_{max} was set to −57% that was obtained by using enantiopure mediator L-**P** as mediator.

interesting that the *syn*/*anti* selectivity is entropic in origin ($T\Delta\Delta S > \Delta\Delta H$ at $T \geq 180$ K), while the enantioselectivity is enthalpically driven ($\Delta\Delta H > T\Delta\Delta S$ at $T \leq 550$ K). These parameters are considered to reflect both the ground-state thermodynamics and the excited-state kinetics (despite the fast intracomplex photoprocess) and hence inappropriate or difficult to attribute to a single step or cause. Nevertheless, the comparable absolute $\Delta\Delta H$ values obtained seem reasonable because the hydrogen-bonding and stacking interactions are the major driving forces and controlling factors of the *syn*/*anti* and enantioselective complexation and subsequent photocyclodimerization, while the more significant contribution of $T\Delta\Delta S$ to the *syn*/*anti* rather than enantioselectivity is more or less related to a larger number of conformational variations that are expected to exist for *anti*- and *syn*-HH precursor complexes than for *re-re* and *si-si* stacked *anti*-HH precursor complexes. Extrapolations of the Eyring plots to further lower temperatures led to an inversion of the *syn*/*anti* selectivity at −122 °C and continued enhancement of the *anti*/*syn* and enantioselectivities to afford *anti*-HH product **3** in 83% yield and −94% ee at −165 °C, if the 2:2 complex is sufficiently soluble to a 3:1 isopentane−methylcyclohexane mixture that does not freeze at that temperature.[17]

Asymmetric Amplification. The dimeric complex structure thus revealed prompted us to explore the "nonlinear effect" or "asymmetric amplification"[18] in this supramolecular photochirogenic system since no such effect has been reported for a photochemical asymmetric reaction.

In a typical asymmetric catalysis, the product's ee (ee_{prod}) is proportional to the ee of catalyst used, being expressed as a product of the maximum product's ee (ee_{max}) obtained by using enantiopure catalyst and the catalyst's ee (ee_{cat}):

$$ee_{prod} = ee_{max} \times ee_{cat} \quad (1)$$

However, if asymmetric amplification (or depletion) occurs via some mechanism, the experimental ee_{prod} is not linear to the ee_{cat} but becomes larger (or smaller) than the value anticipated from eq 1. The present photochirogenic system mediated by a mixture of D- and L-**P** at different ratios can be analyzed by the equation derived for the Kagan's ML_2 model (more strictly the M^*L_2 model) that incorporates two chiral ligands coordinated to a metal center:[18]

$$ee_{prod} = [(1 + \beta)/(1 + g\beta)] \times ee_{max} \times ee_{cat} \quad (2)$$

where β and g, respectively, represent the relative concentration and photocyclodimerization rate constant of heterochiral $\mathbf{A}_2$·L-**P**·D-**P** complex versus homochiral $\mathbf{A}_2$·L-$\mathbf{P}_2$ (and $\mathbf{A}_2$·D-$\mathbf{P}_2$) complex. Thus, if the heterochiral complex is less reactive than the homochiral one, that is, $g < 1$ and hence $(1 + \beta)/(1 + g\beta) > 1$, then the ee_{prod} is greater than any given ee_{cat}, exhibiting the positive nonlinear effect, while the reverse situation leads to the negative nonlinear effect.[18]

In order to examine this possibility, we performed the supramolecular photochirogenesis of **A** (0.25 mM) mediated by mixed L- and D-**P** (0.5 mM in total) of 100, 75, 50, 25, and −50% ee in dichloromethane at −50 °C to obtain the results shown in Table 9. In Figure 12, the normalized product ee, that is, ee_{prod}/ee_{max}, is plotted against the mediator ee (ee_{cat}) to reveal the operation of asymmetric amplification in this prolinol-mediated photochirogenesis, which is driven by preferential homochiral 2:2 complexation ($\beta < 1$) and/or its faster photocyclodimerization ($g < 1$). As shown in Figure 12, the simulation curve assuming $g = 0.45$ (and no preferential complexation; i.e., $K_{22}^{\mathbf{A}_2\cdot\text{L-P}\cdot\text{D-P}} = K_{22}^{\mathbf{A}_2\cdot\text{L-P2}}$) in eq 2 gave a reasonable fit, indicating that the photocyclodimerization is ca. 2-fold faster in a homochiral than in a heterochiral 2:2 complex. The gradually decreasing conversions with lowering ee_{cat} (Table 9) are compatible with the rate equation derived by Blackmond.[19]

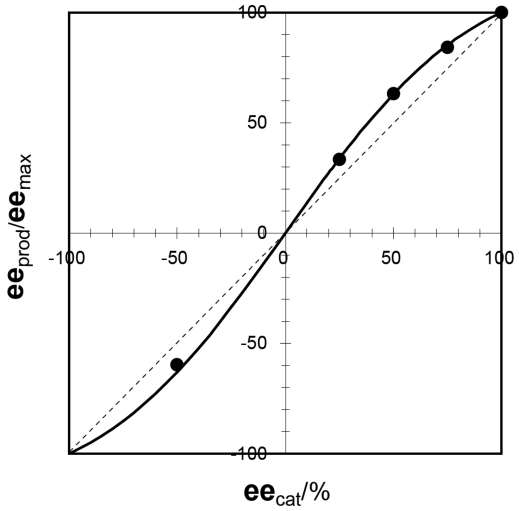

Figure 12. Plot of the normalized product ee (ee_{prod}/ee_{max}) as a function of the mediator ee (ee_{cat}); for the original data, see Table 9. The fitting curve (solid line) is for $g = 0.45$ in eq 2; see the text.

Asymmetric amplification has widely been documented in the literature and mechanistically well understood,[18−20] but the reported examples are limited so far to thermal asymmetric catalysis systems that involve two or more chiral ligands coordinated to metal center(s). In the present study, we have demonstrated for the first time that the photochemical asymmetric amplification is feasible also by using the

DOI: 10.1021/jacs.6b05598
J. Am. Chem. Soc. 2016, 138, 12187−12201

supramolecular photocyclodimerization through a higher-order complex with chiral template.

CONCLUSIONS

In the first part of this study, we demonstrated that simple L-prolinol functions as a versatile template to form not only the stoichiometric 1:1 complex but also the higher-order 1:2, 2:1, and 2:2 complexes with 2-anthracenecarboxylic acid through sophisticated hydrogen-bonding networks. All of the higher-order complexes were experimentally proven to exist and quantitatively analyzed by UV/vis, steady-state and time-correlated fluorescence, CD, NMR, and CSI-MS spectral examinations. The full complexation equilibria and the relevant thermodynamic parameters, as well as the structures and properties of the unprecedented higher-order complexes, were elucidated by combined spectroscopic and theoretical studies. In particular, the structures and relative energies of four stereoisomeric conformers of the 2:2 complex were theoretically predicted by the DTF-D3 and the SCS-MP2 calculations, the results of which were fully compatible with the experimental *syn*/*anti* and enantioselectivities of the HH cyclodimers derived therefrom. This means that we have established the valid experimental and theoretical protocols for comprehensively elucidating the whole m:n (m, $n \leq 2$) supramolecular association behavior.

The photocyclodimerization of 2-anthracenecarboxylic acid was greatly accelerated and made highly stereoselective by forming a 2:2 complex with L-prolinol to give almost exclusively the HH cyclodimers (in >99% yield) and the *P*-enantiomer of **3** in high enantioselectivities (of up to 72% ee) at low temperatures. From the supramolecular photochirogenic viewpoint, the present hydrogen-bonding template strategy conceptually differs from the conventional ones. Thus, the enantiodifferentiation is achieved not by shielding one of the enantiotopic faces of a prochiral substrate but also by assembling two prochiral substrates in an enantiotopic face-selective manner through higher-order complexation with a shieldless template. The intracomplex photoreaction is intrinsically much faster, more efficient and selective, and less quenchable than the intermolecular one, enabling the unprecedented photochemical asymmetric amplification. The higher-order hydrogen-bonding motif may further be exploited for developing new bimolecular photoreactions that are hindered or discouraged by short lifetimes or competing unimolecular processes.

These results and concepts strongly encourage the use of the new hydrogen-bonding motif based on prolinol and β-aminoalcohol as a tool for mediating supramolecular (photo)-chirogenic reactions of single and mixed substrates with asymmetric amplification and more widely for chiroptical sensing and for constructing chiral functional supramolecular architectures after appropriate modifications for the target system.

EXPERIMENTAL SECTION

Instruments. ^{1}H NMR spectra were obtained on a Varian Inova 600 instrument at 600 MHz. Cold-spray ionization mass spectra were measured on a Bruker micrOTOF focus II instrument equipped with a cryospray ionization device by directly injecting a mixture of **A** and **P** dissolved in dichloromethane containing 10% acetonitrile for facilitating ionization. UV/vis spectra were recorded on JASCO V-550 or V-560 spectrophotometer equipped with an ETC-505T temperature controller and CD spectra on JASCO J-720WI or J-820YH spectropolarimeter equipped with a PMH-354WI temperature controller (≥0 °C) or a USP-203HP Unisoku cryostat (<0 °C). Steady-state fluorescence spectra were measured on a JASCO FP-8500 spectrofluorimeter equipped with a USP-203HP Unisoku cryostat. The excitation and emission slits were set at 3 and 1 nm, respectively, and the excitation wavelength was set at 355 nm, one of the isosbestic points observed upon UV/vis spectral titration of **A** with **P** (Figure 1). Fluorescence decay profiles were recorded on an Edinburgh FL 920S instrument equipped with a hydrogen-filled nanosecond flash lamp. The excitation wavelength was set at 355 nm, and the excitation and emission slit widths were set at 10 nm. HPLC analyses were run on JASCO or Shimadzu instrument equipped with a FP-2020SS or RF-20A fluorescence detector.

Materials. 2-Anthracenecarboxylic acid (**A**), (*S*)-2-(hydroxymethyl)pyrrolidine (L-prolinol, **P**), (*S*)-2-(methoxymethyl)-pyrrolidine ($\mathbf{P}_{OM}$), and (*S*)-2-hydroxymethyl-*N*-methylpyrrolidine ($\mathbf{P}_{NM}$) were purchased from Wako and used as received. Fluorescence-free dichloromethane (Aldrich) was used as a solvent throughout the work. Distilled acetonitrile and deionized water were used for the HPLC analysis.

Photoirradiation and Product Analysis. Sample solutions for photoreaction were prepared by mixing stock solutions (2 mL each) of **A** (0.5 mM) and prolinol derivatives, **P** (0.05, 0.125, 0.25, 0.5, 1.0, 2.5, 5.0, and 20 mM), $\mathbf{P}_{NM}$ (2.5 mM), or $\mathbf{P}_{OM}$ (5 mM), and transferred to quartz cells (10 × 10 × 45 mm). After being purged with nitrogen gas for 5 min in an ice bath, the sample was placed in a USP-203HP Unisoku cryostat and irradiated at a given temperature by a 500 W ultra-high-pressure mercury arc fitted with a UV-35 filter (effective λ > 320 nm). The irradiated sample was evaporated under vacuum to give a residue, to which a mixture of aqueous NaOH (2.5 mM) solution and acetonitrile (2 mL each) was added. After filtration, the resulting solution was injected to a chiral HPLC system equipped with a tandem column of Cosmosil 5C18-AR-II (Nacalai) and Chiralcel OJ-RH (Daicel) eluted by a 64:36 mixture of water and acetonitrile containing 0.1% trifluoroacetic acid at 35 °C at a flow rate of 0.5 mL min^{-1}. The product distribution and ee value were determined by integrating the peak area of the chromatogram monitored by a fluorescence detector with excitation and monitoring wavelengths set at 254 and 420 nm, respectively. In the fluorescence detector cuvette, cyclodimers **1**−**4** were efficiently photodecomposed by the excitation light at 254 nm to regenerate **A**, which was immediately photoexcited in the same detector cuvette to emit fluorescence at 420 nm to achieve highly sensitive detection.[21]

Job Analysis. The complexation stoichiometries of **A** with **P**, $\mathbf{P}_{OM}$, and $\mathbf{P}_{NM}$ were examined by the Job analysis using UV/vis and/or CD spectroscopy at a fixed total concentration of 0.25 mM (for $\mathbf{P}_{NM}$) or 0.35 mM (for **P** and $\mathbf{P}_{OM}$). A series of dichloromethane solutions of different molar fractions (x) of **A** at 0.2, 0.3, 0.4, 0.5, 0.6, 0.67, 0.7, 0.8, and 0.9 were prepared for each template and subjected to UV/vis and/or CD spectral examinations at 0 or 25 °C. The intensity changes at the UV/vis spectral peak of the 0−0 band of **A** or the CD spectral extrema were used for constructing the Job plots.

Spectral Titration and Association Constant Determination. Fluorescence, UV/vis, and/or CD spectral titrations were performed at several temperatures to determine the association constants K_{mn} (m, n = 1 or 2) for complexation of **A** with **P**, $\mathbf{P}_{NM}$, and $\mathbf{P}_{OM}$. Fluorescence spectral titration was run by adding a template of 0.1 to 10 or 20 equiv to a dichloromethane solution of **A** at low concentrations (25 and 5 μM) to obtain reliable K_{11} values, while avoiding contamination from the higher-order complexes. The K_{11} values were determined by the nonlinear least-squares fit of the titration data, assuming the 1:1 stoichiometry, by using the Kaleida Graph software.

CD spectral titration was run by adding **P** of 0.25−8 equiv to a dichloromethane solution of **A** (0.1 mM) placed in a quartz cell of 2 mm thickness. The CD spectral titration data obtained were analyzed by the procedures developed on the IGOR Pro software for the equilibria (Scheme 2) to give the association constants for all $\mathbf{A}_m\cdot\mathbf{P}_n$ (m, n = 1 or 2) species in the system. The equilibria shown in Scheme 2 lead to eq 3 for the initial template concentration $[\mathbf{P}]_0$.

DOI: 10.1021/jacs.6b05598
J. Am. Chem. Soc. 2016, 138, 12187−12201

$$[\mathbf{P}]_0 = [\mathbf{P}] + [\mathbf{A}\cdot\mathbf{P}] + 2[\mathbf{A}\cdot\mathbf{P}_2] + [\mathbf{A}_2\cdot\mathbf{P}] + 2[\mathbf{A}_2\cdot\mathbf{P}_2] \quad (3)$$

By replacing the concentration of each complex with those of **A** and **P** and the relevant association constant K_{mn}, we obtain eq 4.

$$2(K_{11}K_{12}[\mathbf{A}] + K_{11}{}^2K_{22}[\mathbf{A}]^2)[\mathbf{P}]^2 + (K_{11}[\mathbf{A}] + K_{11}K_{21}[\mathbf{A}]^2 + 1)[\mathbf{P}] - [\mathbf{P}]_0 = 0 \quad (4)$$

Nonlinear least-squares fit to this equation of the CD spectral titration data obtained at each temperature was performed by using the IGOR procedures with fixed K_{11} (determined independently by the fluorescence titration) to afford the K_{12}, K_{21}, and K_{22} values. The population of each complex species was calculated by using these association constants with the Mathematica software.

Theoretical Calculations. All calculations were performed on Linux-PCs using the TURBOMOLE 6.4 and 6.5 program suites.[22] The resolution of identity approximation was employed in all DFT-D3-B-LYP calculations with a zero-damping function.[23] The basis sets were taken from the TURBOMOLE basis set library. The program modules escf and ricc were used in the TD-DFT and coupled-cluster (CC2) response treatments.

The geometries of $\mathbf{A}_2\cdot\mathbf{P}_2$ conformers were optimized at the DFT-D3-B-LYP/def2-TZVP level with numerical quadrature grid m5. The effect of solvation was incorporated by the conductor-like screening method (COSMO)[14] with the dielectric constant of dichloromethane (ε = 8.93). Single-point energy calculations were performed for all conformer structures by the SCS-MP2 method[15] using a basis set of def2-TZVPP quality with the COSMO solvation model. The relative energy thus obtained enabled calculation of the Boltzmann distribution of each conformer at a given temperature.

■ ASSOCIATED CONTENT

Supporting Information

The Supporting Information is available free of charge on the ACS Publications website at DOI: 10.1021/jacs.6b05598.

UV/vis, CD, and fluorescence spectral titrations and Job plots, fluorescence lifetimes, enthalpy−entropy compensation plots, and optimized structures, atomic coordinates, theoretical CD spectra, and potential energy curves of $\mathbf{A}_2\cdot\mathbf{P}_2$ conformers (PDF)

■ AUTHOR INFORMATION

Corresponding Author

*inoue@chem.eng.osaka-u.ac.jp

Notes

The authors declare no competing financial interest.

■ ACKNOWLEDGMENTS

This work was supported by grants from JSPS (Nos. JP21245011, JP26620030, JP15H03779, JP15K13642, and JP15H01087), JST (MP27215667549), MEXT (Management Expenses Grants for National Universities Corporations), National Natural Science Foundation of China (Nos. 21372165, 21321061, 21402129, and 21572142), State Key Laboratory of Polymer Materials Engineering (sklpme 2014-2-06), and Comprehensive Training Platform of Specialized Laboratory (College of Chemistry, Sichuan University), all of which are gratefully acknowledged.

■ REFERENCES

(1) (a) Rau, H. *Chem. Rev.* **1983**, *83*, 535. (b) Inoue, Y. *Chem. Rev.* **1992**, *92*, 741. (c) Griesbeck, A. G.; Meierhenrich, U. J. *Angew. Chem., Int. Ed.* **2002**, *41*, 3147. (d) Inoue, Y., Ramamurthy, V., Eds. *Chiral Photochemistry*; Marcel Dekker: New York, 2004.

(2) (a) Grosch, B.; Bach, T. Template-Induced Enantioselective Photochemical Reactions in Solution. In *Chiral Photochemistry*; Inoue, Y., Ramamurthy, V., Eds.; Marcel Dekker: New York, 2004. (b) Wada, T.; Inoue, Y. Supramolecular Asymmetric Photoreactions. In *Chiral Photochemistry*; Inoue, Y., Ramamurthy, V., Eds.; Marcel Dekker: New York, 2004. (c) Ramamurthy, V.; Sivaguru, J.; Shailaja, J.; Natanjan, A.; Kaanumalle, L. S.; Karthikeyan, S.; Joy, A. Chiral Photochemistry within Zeolites. In *Chiral Photochemistry*; Inoue, Y., Ramamurthy, V., Eds.; Marcel Dekker: New York, 2004. (d) Müller, C.; Bach, T. *Aust. J. Chem.* **2008**, *61*, 557. (e) Yang, C.; Inoue, Y. Supramolecular Photochirogenesis. In *Supramolecular Photochemistry*; Ramamurthy, V., Inoue, Y., Eds.; Wiley: Hoboken, NJ, 2011; pp 115−154. (f) Yang, C. *Chin. Chem. Lett.* **2013**, *24*, 437. (g) Yang, C.; Inoue, Y. *Chem. Soc. Rev.* **2014**, *43*, 4123.

(3) (a) Bach, T.; Bergmann, H.; Harms, K. *Angew. Chem., Int. Ed.* **2000**, *39*, 2302. (b) Bach, T.; Bergmann, H.; Grosch, B.; Harms, K. *J. Am. Chem. Soc.* **2002**, *124*, 7982. (c) Bauer, A.; Westkämper, F.; Grimme, S.; Bach, T. *Nature* **2005**, *436*, 1139. (d) Müller, C.; Bauer, A.; Maturi, M. M.; Cuquerella, C.; Miranda, M. A.; Bach, T. *J. Am. Chem. Soc.* **2011**, *133*, 16689. (e) Coote, S. C.; Bach, T. *J. Am. Chem. Soc.* **2013**, *135*, 14948. (f) Maturi, M. M.; Fukuhara, G.; Tanaka, K.; Kawanami, Y.; Mori, T.; Inoue, Y.; Bach, T. *Chem. Commun.* **2016**, *52*, 1032.

(4) Gerard, B.; Sangji, S.; O'Leary, D. J.; Porco, J. A. *J. Am. Chem. Soc.* **2006**, *128*, 7754.

(5) Cauble, D. F.; Lynch, V.; Krische, M. J. *J. Org. Chem.* **2003**, *68*, 15.

(6) (a) Mizoguchi, J.; Kawanami, Y.; Wada, T.; Kodama, K.; Anzai, K.; Yanagi, T.; Inoue, Y. *Org. Lett.* **2006**, *8*, 6051. (b) Kawanami, Y.; Pace, T. C. S.; Mizoguchi, J.; Yanagi, T.; Nishijima, M.; Mori, T.; Wada, T.; Bohne, C.; Inoue, Y. *J. Org. Chem.* **2009**, *74*, 7908. (c) Kawanami, Y.; Katsumata, S.; Mizoguchi, J.; Nishijima, M.; Fukuhara, G.; Yang, C.; Mori, T.; Inoue, Y. *Org. Lett.* **2012**, *14*, 4962. (d) Kawanami, Y.; Umehara, H.; Mizoguchi, J.; Nishijima, M.; Fukuhara, G.; Yang, C.; Mori, T.; Inoue, Y. *J. Org. Chem.* **2013**, *78*, 3073.

(7) Vallavoju, N.; Selvakumar, S.; Jockusch, S.; Sibi, M. P.; Sivaguru, J. *Angew. Chem., Int. Ed.* **2014**, *53*, 5604.

(8) Mayr, F.; Brimioulle, R.; Bach, T. *J. Org. Chem.* **2016**, *81*, 6965.

(9) (a) Wakai, A.; Fukasawa, H.; Yang, C.; Mori, T.; Inoue, Y. *J. Am. Chem. Soc.* **2012**, *134*, 10306; **2012**, *134*, 4990. (correction) (b) Kawanami, Y.; Tanaka, H.; Mizoguchi, J.; Kanehisa, N.; Fukuhara, G.; Nishijima, M.; Mori, T.; Inoue, Y. *Acta Crystallogr., Sect. C: Cryst. Struct. Commun.* **2013**, *C69*, 1411.

(10) (a) Werner, T. C.; Hercules, D. M. *J. Phys. Chem.* **1970**, *74*, 1030. (b) Nakamura, A.; Inoue, Y. *J. Am. Chem. Soc.* **2003**, *125*, 966.

(11) Rekharsky, M. V.; Inoue, Y. *Chem. Rev.* **1998**, *98*, 1875.

(12) (a) Sakamoto, S.; Fujita, M.; Kim, K.; Yamaguchi, K. *Tetrahedron* **2000**, *56*, 955. (b) Yamaguchi, K. *J. Mass Spectrom.* **2003**, *38*, 473.

(13) (a) Wendler, K.; Thar, J.; Zahn, S.; Kirchner, B. *J. Phys. Chem. A* **2010**, *114*, 9529. (b) Grimme, S.; Antony, J.; Ehrlich, S.; Krieg, H. *J. Chem. Phys.* **2010**, *132*, 154104.

(14) Klamt, A.; Jonas, V. *J. Chem. Phys.* **1996**, *105*, 9972.

(15) (a) Grimme, S. *J. Chem. Phys.* **2003**, *118*, 9095. (b) Grimme, S. *J. Phys. Chem. A* **2005**, *109*, 3067.

(16) (a) Yang, C.; Fukuhara, G.; Nakamura, A.; Origane, Y.; Fujita, K.; Yuan, D.-Q.; Mori, T.; Wada, T.; Inoue, Y. *J. Photochem. Photobiol., A* **2005**, *173*, 375. (b) Nakamura, A.; Inoue, Y. *J. Am. Chem. Soc.* **2005**, *127*, 5338.

(17) (a) Murov, S. L. *Handbook of Photochemistry*; Marcel Dekker: New York, 1973. (b) Greenspan, H.; Fischer, E. *J. Phys. Chem.* **1965**, *69*, 2466.

(18) Girard, C.; Kagan, H. B. *Angew. Chem., Int. Ed.* **1998**, *37*, 2922.

(19) Blackmond, D. *Acc. Chem. Res.* **2000**, *33*, 402.

(20) Inanaga, J.; Furuno, H.; Hayano, T. *Chem. Rev.* **2002**, *102*, 2211.

(21) Nishijima, M.; Wada, T.; Nagamori, K.; Inoue, Y. *Chem. Lett.* **2009**, *38*, 726.

DOI: 10.1021/jacs.6b05598
J. Am. Chem. Soc. 2016, 138, 12187−12201

(22) *TURBOMOLE* V6.4 and 6.5, product of University of Karlsruhe and Forschungszentrum Karlsruhe GmbH in 1989−2007 and of TURBOMOLE GmbH since 2007; http://www.turbomole.com.
(23) (a) Liu, Y.; Goddard, W. A., III *Mater. Trans.* **2009**, *50*, 1664. (b) Moellmann, J.; Grimme, S. *Phys. Chem. Chem. Phys.* **2010**, *12*, 8500. (c) Hujo, W.; Grimme, S. *Phys. Chem. Chem. Phys.* **2011**, *13*, 13942.

DOI: 10.1021/jacs.6b05598
J. Am. Chem. Soc. 2016, 138, 12187−12201